Modeling Photosynthesis and Exudation in Subtropical Oceans

Global Biogeochemical Cycles®

RESEARCH ARTICLE
10.1029/2021GB006941

Key Points:

- Decoupling of photosynthesis and biosynthesis improved simulations of primary production
- Predicted global primary production increased by about 1/3
- Model results suggest exudation could contribute ~20% to total dissolved organic carbon fluxes in euphotic layer

Supporting Information:

Supporting Information may be found in the online version of this article.

Correspondence to:

Z. Wu,
zhenwu@mit.edu

Citation:

Wu, Z., Dutkiewicz, S., Jahn, O., Sher, D., White, A., & Follows, M. J. (2021). Modeling photosynthesis and exudation in subtropical oceans. *Global Biogeochemical Cycles*, *35*, e2021GB006941. https://doi.org/10.1029/2021GB006941

Received 12 JAN 2021
Accepted 4 SEP 2021

Modeling Photosynthesis and Exudation in Subtropical Oceans

Zhen Wu[1], Stephanie Dutkiewicz[1], Oliver Jahn[1], Daniel Sher[2], Angelicque White[3], and Michael J. Follows[1]

[1]Department of Earth, Atmospheric and Planetary Sciences, Massachusetts Institute of Technology, Cambridge, MA, USA, [2]Department of Marine Biology, Leon H. Charney School of Marine Sciences, University of Haifa, Haifa, Israel, [3]Department of Oceanography, University of Hawaii at Manoa, Honolulu, HI, USA

Abstract Marine phytoplankton contributes nearly half of the total primary production on Earth through photosynthesis. Parameterizations of algal photosynthesis commonly employed in global biogeochemical simulations generally fail to capture the observed vertical structure of primary production. Here we examined the consequences of decoupling photosynthesis (carbon fixation) and biosynthesis (biomass building) with accumulation or exudation of excess photosynthate under energy rich conditions in both regional and global models. The results show that the decoupling of these two processes improved the simulated vertical profile of primary production, increased modeled primary production over 30% globally and over 40% in subtropical oceans, improved simulated meridional patterns of particulate C:N:P and increased modeled surface pool of labile/semi-labile dissolved organic carbon. More generally, these results highlight the importance of exudation, which results from the decoupling of photosynthesis and biosynthesis, as a major physiological process affecting ocean biogeochemistry.

1. Introduction

The structure and rates of photosynthesis and biosynthesis by primary producers in the ocean's subtropical gyres reflect the balance between photons delivered from above, macro-nutrients delivered largely from below, and essential trace metals such as iron which has both oceanic and atmospheric sources. The observed vertical profiles in Figure 1 from North Pacific and North Atlantic subtropical gyres (Karl & Church, 2014; Letelier et al., 1996; Steinberg et al., 2001; White et al., 2015) reveal the transition from nutrient to light limitation over a relatively short distance (less than 100 m). The vertical gradients of light and fixed nitrogen oppose one another in the upper ocean (Figure 1) suggesting an excess supply of energy near the surface. However primary production also increases toward the surface raising the question of how organisms are balancing carbon, energy and nutrient supply and demand.

Phytoplankton may balance the supply and demand of photosynthesis and biosynthesis by the regulation of nutrient uptake (Flynn, 2003), "luxury storage" of resources in excess of demand (Martin et al., 2014), photo-respiration (Beardall et al., 2003) or the exudation of excess photosynthate (Halsey & Jones, 2015). Photo-respiration is reported to be significant only in CO_2 depleted regions which should be minimal in the euphotic zone (Beardall, 1989; Beardall et al., 2003; Colman, 1989). The excretion of dissolved organic carbon (DOC) in nutrient replete, exponentially growing phytoplankton is low, ~2% of total gross carbon fixation (López-Sandoval et al., 2013). However, recent studies show that *Prochlorococcus*, an abundant pico-cyanobacterium found in oligotrophic ocean regions and which only have a moderate ability for photoacclimation, can excrete a large fraction of fixed C under nutrient-limited conditions (Bertlisson et al., 2005; Cailliau et al., 1996; Kulk et al., 2011; Roth-Rosenberg et al., 2021; Szul et al., 2019; Thompson et al., 2018). Thus exudation is more likely significant in the oligotrophic surface ocean where there is persistent nutrient limitation and light-saturating conditions. The exudates may be a source of carbon for heterotrophic bacteria (Berman & Holm-Hansen, 1974; Bjørrisen, 1988), increasing the total biomass of bacteria, enhancing remineralization, and promoting the co-evolution of phototrophic and heterotrophic populations (Braakman et al., 2017; Sarmento et al., 2016).

Most biogeochemical models treat photosynthesis and biosynthesis as a single process, and many do not take into account DOC exudation. Physiologically, photosynthesis can be limited by the availability of light and photosynthetic apparatus (Mackey et al., 2008; Letelier et al., 2017), while biosynthesis is limited by the

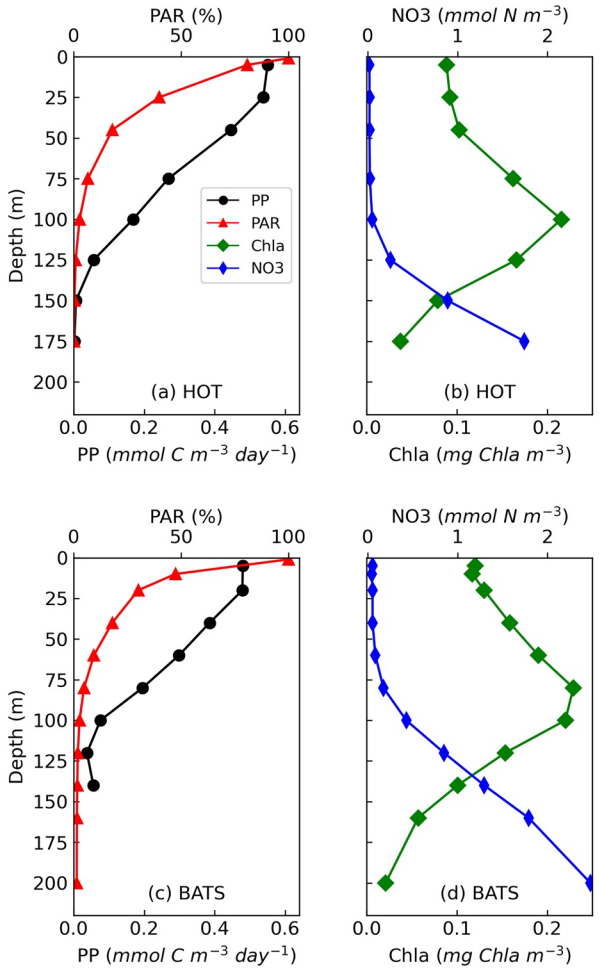

Figure 1. Observed climatological average of photosynthesis rate, Chla, nitrate, and photosynthetically active radiation (PAR) at Hawaii Ocean Time-series (HOT) and Bermuda Atlantic Time-Series (BATS). The data were obtained from the observations from 1988 to 2018 at both stations.

external availabilities and cellular reserves of nitrogen (N), phosphorus (P), or iron (Fe) (Halsey & Jones, 2015; Marañón et al., 2013) as well as the necessary self-replicating apparatus. Thus, models that treat the two as a single process will possibly underestimate photosynthesis by imposing nutrient limitation on it. Some models have included DOC exudation either as a simple fraction of primary production or by linking exudation to nutrient limitation, biomass, and nutrient stoichiometry (Grossowicz et al., 2017; Schartau et al., 2007; Vallino, 2000; Xiu & Chai, 2014), see review by Livanou et al. (2019). The essence of these models is to compare the cellular carbon and nutrient reserves which are constrained by photosynthesis and nutrient uptakes in similar stoichiometric ratios as structural components. The minimal cellular reserve limits the rate of biosynthesis. Besides the cost of biosynthesis, extra carbon or other nutrients in these reserves may be exuded into the environment. However even these models likely underestimate photosynthesis as they still include nutrient limitation on this process.

In this study we use numerical models to investigate the consequences of parameterizing photosynthesis and biosynthesis separately, removing the nutrient limitation on photosynthesis, and allowing exudation of DOC. We consider how these modification affect the simulation of primary production in the oligotrophic gyres, as well as the global rates of photosynthesis and potential rates of DOC exudation. We first implemented this parameterization to vertical 1-Dimensional (1D) models at Hawaii Ocean Time-series (HOT) in the North Pacific Subtropical Gyre and Bermuda Atlantic Time-Series (BATS) in the North Atlantic focusing on the vertical profiles of primary production. And we then applied this parameterization to a 3-Dimensional (3D) configuration to estimate the changes of global primary production. We find that removing direct macronutrient limitation on photosynthesis, but retaining the indirect cost of maintaining photosynthetic machinery, significantly improves the vertical structure and vertically integrated rates of primary production in both 1D and 3D simulations. It also increases global primary production and DOC production by about 30% in a 3D global model.

In the study that follows, our primary goal is to illustrate that relieving a strong, direct nutrient limitation constraint on a model of photosynthesis significantly improves simulations of the vertical structure of photosynthesis in the subtropical ocean with the consequence of significantly increasing simulated global, annual primary production. The parameterization requires the production of excess photosynthate which, consistent with empirical evidence, is either accumulated in particles or exuded as DOC. The subsequent and overall controls of particulate C:N:P and DOC distributions are complex and the subject of significant ongoing study, and so are not the main focus of this work.

2. Methods

2.1. Environmental Modeling Framework

The biogeochemical-ecosystem model used here describes the cycling of carbon, nitrogen, phosphorus, iron, silica and oxygen in both living and non-living forms as discussed in Dutkiewicz et al. (2015) and Follows et al. (2007). We employ 1D and 3D physical configurations with identical biogeochemistry and ecology. We first examine the qualitative impact of decoupling carbon and nutrient flows in vertically well-resolved 1D simulations, focusing specifically on the alterations to the vertical changes in primary production, and then scale up to consider the global impact in 3D simulations, focusing more on the regional and global responses.

The 1D simulations were configured to resolve only the vertical dimension in space. The 6,000 m deep column has a vertical resolution of 10 m from sea surface to 120 m depth and with gradually increasing thickness thereafter. Nutrient distributions and plankton biomass were initialized according to World Ocean Atlas (Garcia et al., 2018) and previous 3D simulations relevant to HOT in the North Pacific Subtropical Gyre and BATS in the North Atlantic (Dutkiewicz et al., 2015). In this configuration, a seasonal mixed layer was driven by restoring to climatological, seasonal sea surface temperatures which drives winter-time convection following Hickman et al. (2010). The 1D framework does not resolve the contributions of isopycnal nutrient transport nor the effect of mesoscale motions, tides, and internal waves which drive intermittent nutrient transfer into the euphotic zone (McGillicuddy, 2016). Hence, the vertical, diapycnal diffusivity for HOT and BATS was modified to parameterize these processes. The time step of 1D configuration is 1 h and we integrate the 1D configuration for 30 years with a repeating generic "year" of external forcings. The model results establish a repeating pattern after several years spin-up leading to a "quasi-steady state" by year 10. In the analysis presented below we consider the climatology of the last 15 years of 30 years simulations.

The 3D configuration of the MIT general circulation model (MITgcm) (Marshall et al., 1997) has a horizontal resolution of $1° \times 1°$. There are 23 vertical levels, 10 m for the top two levels, and then graduated in thickness to 500 m at depth. The physical fields are constrained by satellite and in-situ observations (Wunsch & Heimbach, 2007) (the ECCO-GODAE state estimate), which is used by many previous biogeochemical-ecosystem studies (Dutkiewicz et al., 2015; Follows et al., 2007; Ward & Follows, 2016; Ward et al., 2012). The 3D simulations were initialized by World Ocean Atlas (Garcia et al., 2018) for nitrate, phosphate, and silicic acid and previous model output (Dutkiewicz et al., 2020) for iron, ammonium, nitrite, dissolved and particulate matter, and plankton biomass. We integrate the system forward in time for 10 years from initial conditions provided by an earlier simulation. The simulated phytoplankton establish a repeating pattern after about 4 years after which the system represents a "quasi-steady state" with a slow, longer term adjustment in nutrient fields not affecting the results that we discuss here. We show results from the tenth year of the simulation.

We resolve two size classes of phytoplankton (picophytoplankton and all others) as well as two types of grazers. The biogeochemical and biological tracers interact through the formation, transformation, and remineralization of organic matter. Mortality, sloppy feeding, and exudation transfer living organic material into sinking particulate and dissolved organic detritus which are respired back to inorganic form with simple parameterizations of the activity of heterotrophic decomposers. Here we resolve a single DOC pool with average life-span of one month. This pool should thus be thought of as a combination of the labile and semi-labile pools (see Text S2 for details). We do not resolve the longer life-time refractory pool. Iron cycling includes scavenging by particles and explicit complexation with an organic ligand following Dutkiewicz et al. (2015). Aeolian iron fluxes to the ocean surface are provided by Luo et al. (2008). The complete model equations and descriptions are provided in the Supporting Information S1.

2.2. Cellular Stoichiometry and Photosynthesis

In this study, we examine the biogeochemical implications of decoupling carbon and nutrient flow by comparing two physiological parameterizations (see Figure 2). In the "coupled model" (depicted in Figure 2a) following Equation 1 (Geider et al., 1997), photosynthesis is directly influenced by the external concentration of fixed nitrogen (proportional to $[NO_3^-] / ([NO_3^-] + K_{NO_3})$). In the "decoupled model," (depicted in Figure 2b) carbon and nitrogen flows are buffered by independent reserves (following, e.g., Bruggeman & Kooijman, 2007; Talmy et al., 2014) and the light-saturated photosynthesis rate for phytoplankton type j, $P_{C,j}^{Sat}$ $(mmol\ C\ (mmol\ C)^{-1}\ d^{-1})$, is not directly dependent on the external fixed-nitrogen availability (Equation 3 compared to Equation 1, Figure S1a):

$$P_{C,j}^{Sat} = P_{C,j}^{max} \frac{R}{R + K_{R,j}} \cdot T_{func} \tag{1}$$

$$T_{func} = \tau \cdot exp\left[A_E \left(\frac{1}{T + 273.15} - \frac{1}{T_0} \right) \right] \tag{2}$$

Following Geider et al. (1997), $P_{C,j}^{max}$ is the maximum carbon-normalized photosynthesis rate of phytoplankton j $(mmol\ C\ (mmol\ C)^{-1}\ d^{-1})$. An explicit accounting of nutrient limitation is represented as a

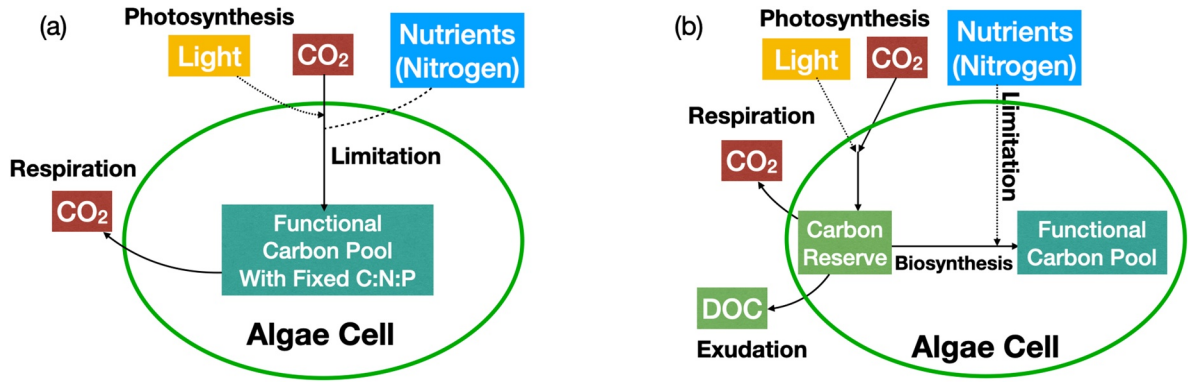

Figure 2. Schematic representations of cellular C flow. (a) represents the model in which C and N flow are tightly coupled. (b) represents the model in which C and N flow are decoupled.

multiplicative, hyperbolic function of R, the limiting nutrient concentration, which throttles back photosynthesis in low nutrient environments with the consequence of tightly coupling photosynthesis and biosynthesis. The temperature dependence is introduced through a multiplicative function T_{func} (Equation 2), where τ is Arrhenius coefficient, A_E is the slope of the linear region of the Arrhenius plot, T_0 is the reference temperature of phytoplankton j (K), and T is water column temperature (°C).

$$P_{C,j}^{Sat} = P_{C,j}^{max} \cdot T_{func} \tag{3}$$

Here nutrient availability only affects photosynthesis through the synthesis of Chla which is controlled by the rate of biosynthesis. Biosynthesis is controlled by the availability of reserves of both photosynthate and other nutrient elements. In the decoupled model, the rate of photosynthesis continues to be controlled by the light environment even when biosynthesis is nitrogen limited. In that case, excess photosynthate is stored in the reserve or exuded. The carbon-specific light limited photosynthesis rate for phytoplankton type j, $P_{C,j}$ $(mmol\ C\ (mmol\ C)^{-1}\ d^{-1})$, is describe below:

$$P_{C,j} = P_{C,j}^{Sat}\left[1 - exp\left(-\frac{\alpha I\ \theta_j}{P_{C,j}^{Sat}}\right)\right] \tag{4}$$

where, α is the initial slope of the photosynthesis-irradiance curve normalized to Chla $(m^2\ (mg\ Chla)^{-1}\ mmol\ C\ (\mu mol\ photons)^{-1})$, I is the flux of photosynthetically active radiation (PAR, $\mu mol\ photons\ m^{-2}\ s^{-1}$), θ_j is the Chla:C ratio of phytoplankton type j ($mg\ Chla\ (mmol\ C)^{-1}$, also in Figure S1b). Please note that photoinhibition and maintenance respiration are not included in both of the two parameterizations since the focus is the comparison between these two parameterizations and we treat photosynthesis as net primary production throughout.

2.3. Details of Physiological Parameterizations

Photosynthate is delivered to a "reserve" (carbohydrate or lipid) from where it may be used for biosynthesis or exuded. The potential rates of uptake of nutrients other than carbon (nitrogen, phosphorus, and iron) are evaluated with Michaelis-Menten kinetics and an Arrhenius temperature dependence, following Equations 5 and 6.

$$V_{R,j} = V_{R,j}^{max} \cdot \gamma_{R,j} \cdot T_{func} \tag{5}$$

$$\gamma_{R,j} = \frac{R}{R + K_{R,j}} \tag{6}$$

where $V_{R,j}^{max}$ is the maximum carbon-normalized uptake rate for resource R of phytoplankton j $(mmol\ R\ (mmol\ C)^{-1}\ d^{-1})$, $\gamma_{R,j}$ is the nutrient limitation based on Michaelis-Menten kinetics, $K_{R,j}$ is the half-saturation concentration of resource R of phytoplankton j $(mmol\ R\ m^{-3})$. The total potential uptake of nitrogen is defined as the sum of the uptake of each species in Equation 7.

$$V_{N,j} = V_{NH_4,j} + V_{NO_3,j} + V_{NO_2,j} \tag{7}$$

Table 1
Biological Parameters of Different Phytoplankton Functional Types

Parameter	Symbol	Type I	Type II	Unit
Maximum photosynthesis rate	P_C^{max}	0.76	3.15	$mmol\ C\ (mmol\ C)^{-1}\ d^{-1}$
Maximum uptake rate	$V_{NO_3}^{max}$	0.49	0.14	$mmol\ N\ (mmol\ C)^{-1}\ d^{-1}$
	$V_{NO_2}^{max}$	0.49	0.14	$mmol\ N\ (mmol\ C)^{-1}\ d^{-1}$
	$V_{NH_4}^{max}$	0.24	0.07	$mmol\ N\ (mmol\ C)^{-1}\ d^{-1}$
	$V_{PO_4}^{max}$	0.014	0.01	$mmol\ P\ (mmol\ C)^{-1}\ d^{-1}$
	V_{Fe}^{max}	1.83×10^{-5}	9.92×10^{-6}	$mmol\ Fe\ (mmol\ C)^{-1}\ d^{-1}$
Half-saturation concentration	K_{NO_3}	2.76×10^{-3}	0.41	$mmol\ N\ m^{-3}$
	K_{NO_2}	2.76×10^{-3}	0.41	$mmol\ N\ m^{-3}$
	K_{NH_4}	1.38×10^{-3}	0.21	$mmol\ N\ m^{-3}$
	K_{PO_4}	1.73×10^{-4}	0.026	$mmol\ P\ m^{-3}$
	K_{FeT}	1.73×10^{-7}	2.59×10^{-5}	$mmol\ Fe\ m^{-3}$
Celluar stoichiometric ratios	$R_{C:N}$	7.5	7.5	$mmol\ C\ (mmol\ N)^{-1}$
	$R_{C:P}$	120.0	120.0	$mmol\ C\ (mmol\ P)^{-1}$
	$R_{C:Fe}$	1.2×10^{5}	1.2×10^{5}	$mmol\ C\ (mmol\ Fe)^{-1}$

The carbon demand to build biomass, $D_{i,j}$ $(mmol\ C\ (mmol\ C)^{-1}\ d^{-1})$, for each nutrient element and each phytoplankton type j, is evaluated based on an assumed, fixed stoichiometry of functional biomass (e.g., protein, nucleic acids, etc) in Equation 8.

$$D_{i,j} = V_{i,j} \cdot R_j^{C:i} \tag{8}$$

where denotes N, P, Fe, $R_j^{C:i}$ is the $C:i$ ratio in phytoplankton j $(mmol\ C\ (mmol\ i)^{-1})$. The carbon-specific production of functional biomass (biosynthesis) is then determined as the minimum of the photosynthesis rate and the carbon demand of the most limiting nutrient in Equations 9 and 10.

$$BS_{C,j} = min[D_{min,j}, P_{C,j}] \tag{9}$$

$$D_{min,j} = min[D_{N,j}, D_{P,j}, D_{Fe,j}] \tag{10}$$

Here we assume that if the net carbon-specific photosynthesis rate is greater than biosynthesis rate (which means biosynthesis is limited by nutrients rather than light energy), a fraction of the excess photosynthate accumulates in the carbon reserve and the remainder $f_{e,j}$ is assumed exuded into the environment as labile/semi-labile DOC at the rate of $E_{C,j}$ $(mmol\ C\ (mmol\ C)^{-1}\ d^{-1})$ as described in Equation 11. In the results we assume $f_{e,j} = 0.7$ in Figures 4–6. We examine this choice later in this manuscript.

$$E_{C,j} = max[0.0, P_{C,j} - BS_{C,j}] \cdot f_{e,j} \tag{11}$$

We parameterize the two classes of phytoplankton as pico-phytoplankton (type I) with high nutrient affinity, but low growth rates, and the larger phytoplankton (type II) with lower nutrient affinity and higher growth (Follows et al., 2007). Values of the parameters (Table 1) are similar to the cyanobacteria and diatom values used in Dutkiewicz et al. (2020). The two phytoplankton types are assumed to have the same basal C:N:P, though we note that it is likely that more opportunistic species have a lower N:P than cyanobacteria (Arrigo, 2005; Mills & Arrigo, 2010).

3. Results and Discussion

First we examine the qualitative impact of decoupling carbon and nutrient flows on the vertical structure of modeled primary production in a 1D framework, referencing observed profiles at HOT and BATS. Then we examine the quantitative impact on integrated primary production in 3D global simulations. For this discussion, we will refer to the simulations in which N and C flow are tightly coupled as the "coupled" simulations and those in which N and C flow are decoupled as the "decoupled" simulations.

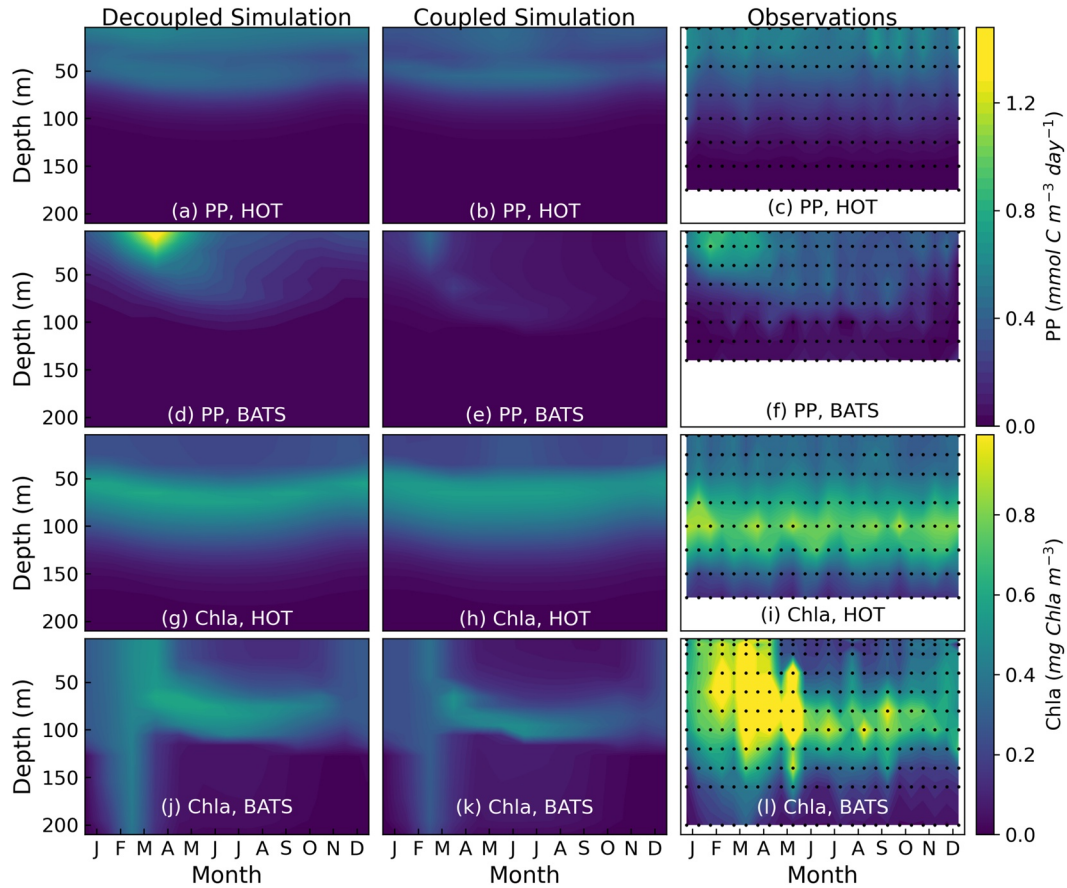

Figure 3. Seasonal variation of photosynthesis rate and Chla at Hawaii Ocean Time-series (HOT) and Bermuda Atlantic Time-Series (BATS). Black dots in the panels of observations indicate the time and depth of the observation. (a) photosynthesis rate of decoupled simulation at station ALOHA ($mmol\ C\ m^{-3}\ d^{-1}$); (b) photosynthesis rate of coupled simulation at station ALOHA ($mmol\ C\ m^{-3}\ d^{-1}$); (c) observed photosynthesis rate at station ALOHA ($mmol\ C\ m^{-3}\ d^{-1}$); (d) photosynthesis rate of decoupled simulation at station Bermuda ($mmol\ C\ m^{-3}\ d^{-1}$); (e) photosynthesis rate of coupled simulation at station Bermuda ($mmol\ C\ m^{-3}\ d^{-1}$); (f) observed photosynthesis rate at station Bermuda ($mmol\ C\ m^{-3}\ d^{-1}$); (g) Chla concentration of decoupled simulation at station ALOHA ($mg\ Chla\ m^{-3}$); (h) Chla concentration of coupled simulation at station ALOHA ($mg\ Chla\ m^{-3}$); (i) observed Chla concentration at station ALOHA ($mg\ Chla\ m^{-3}$); (j) Chla concentration of decoupled simulation at station Bermuda ($mg\ Chla\ m^{-3}$); (k) Chla concentration of coupled simulation at station Bermuda ($mg\ Chla\ m^{-3}$); (l) observed Chla concentration at station Bermuda ($mg\ Chla\ m^{-3}$).

3.1. Vertical Profiles of Subtropical Productivity

We first examine qualitative differences between 1D simulations where photosynthesis is explicitly limited by nutrient concentrations following Equation 1 ("coupled" model, Figure 2a, nutrient profiles showed in Figures S2 and S3) to simulations where nutrients only affect photosynthesis through the synthesis of photosynthetic pigments ("decoupled" model, Figure 2b, also see Equations S20 and S21). The climatologies of the last 15 years of the simulations are compared with climatological data from HOT (1988–2018) and BATS (1989–2016). Some general features of the two sites were qualitatively captured in both simulations (Figure 3) including the late winter bloom at BATS and the DCM at both sites (during the summer at BATS and year-round at HOT), and plausible nutrient distributions (Figures S2 and S3). As observed, simulated seasonality at HOT was much weaker than at BATS due to the difference in seasonal physical forcing (Cavender-Bares et al., 2001; Karl & Church, 2014; Malmstrom et al., 2010; Steinberg et al., 2001).

However, the coupled and decoupled simulations also show some significant differences with one-another which we highlight in Figure 4. Due to the explicit throttling back of photosynthesis in the highly oligotrophic surface waters caused by nutrient limitation, the coupled model fails to capture the increase of

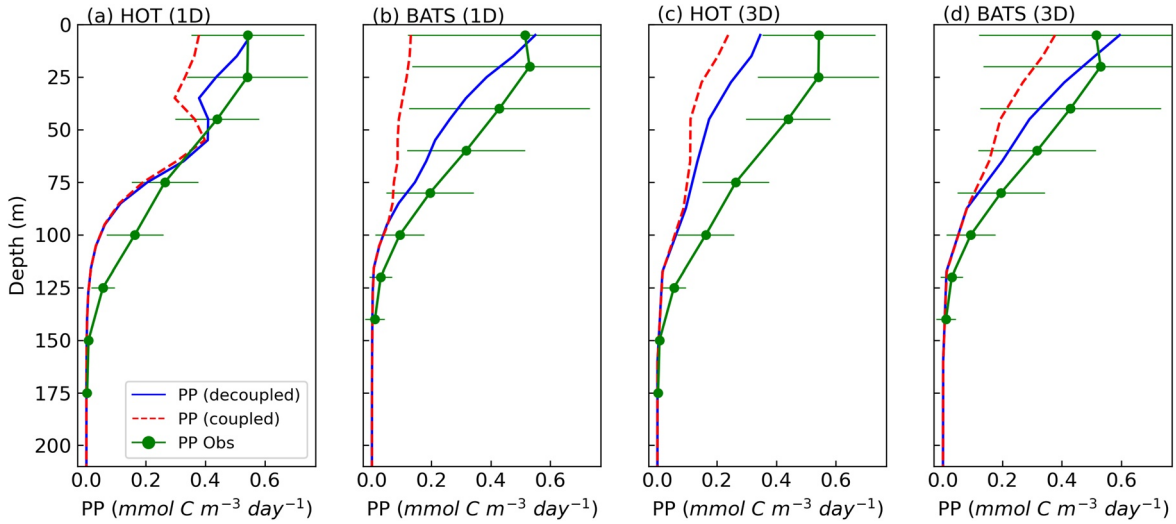

Figure 4. Annual averaged vertical profiles of primary production at Hawaii Ocean Time-series (HOT) and Bermuda Atlantic Time-Series (BATS) in both 1-Dimensional (1D) and 3-Dimensional (3D) simulations. Model results are annual averages from the last 15 years of 30 years integration in 1D simulations and the 10th year integration in 3D simulations. The green solid lines indicate observed primary production from 1988 to 2016 and the horizontal green bars represent deviation of the inter-annual variations. The red dashed lines indicate the coupled simulation, where photosynthesis is directly regulated by local nutrient concentration. The blue solid lines represent simulations of photosynthesis rate in the decoupled simulation.

photosynthesis toward the surface both at HOT and, more strikingly, at BATS. The coupled model consistently predicts extremely low photosynthesis rates near the surface relative to the observed climatologies. In contrast, the solid blue lines in Figure 4 indicate the simulations of the decoupled model. Here photosynthesis was not throttled back under low nitrogen conditions however nitrogen limitation does control biosynthesis of pigments. The vertical profiles of primary production increase toward the surface, both qualitatively and quantitatively more consistent with the observations.

The vertically integrated rate of photosynthesis (0–200 m) in the 1D decoupled simulation is increased by ~ 21.1% at HOT and more than 170% at BATS compared to the coupled simulation. In the upper 200 m of the 1D decoupled simulations, photosynthesis exceeded biosynthesis rate by ~25% at HOT and ~58% at BATS. Excess photosynthate in the decoupled simulations accumulates as storage in the cells or is exuded, consistent with numerous laboratory and field studies (Bjørrisen, 1988; Szul et al., 2019; Thornton, 2014). The general consequences of the balance between storage and exudation for the C:N:P ratio of phytoplankton biomass and production of DOC are examined in the following 3D study.

3.2. Global Biomass and Productivity

In the previous section we demonstrated that the decoupling of N and C flow in the physiological model leads to a significant qualitative improvement in simulations of primary production, focusing specifically on the vertical response using a 1-D model with high vertical resolution. We now consider how the decoupling of C and N in photosynthesis will impact regionally and alter global primary production and elemental composition of phytoplankton (and particulate matter) within a three dimensional model. We note here that due to the physical setup of the three dimensional model, the vertical is not resolved as well as in the 1-D model.

Both coupled and decoupled simulations capture the high surface Chla, primary production, and nutrient concentrations in the subpolar and equatorial regimes, as well as low surface Chla, primary production, and nutrient concentrations in subtropical gyres (Figure 5, also see Figure S4). Typical for such coarse resolution simulations, the dynamics and biogeochemistry of continental shelves and coastal regions are not resolved or well represented. Moreover, the coarse resolution does not capture mesoscale features which are important in mediating nutrient supply in the subtropical regions (Clayton et al., 2013; McGillicuddy, 2016), and both Chl-a and primary production are lower in the model than found in the real ocean.

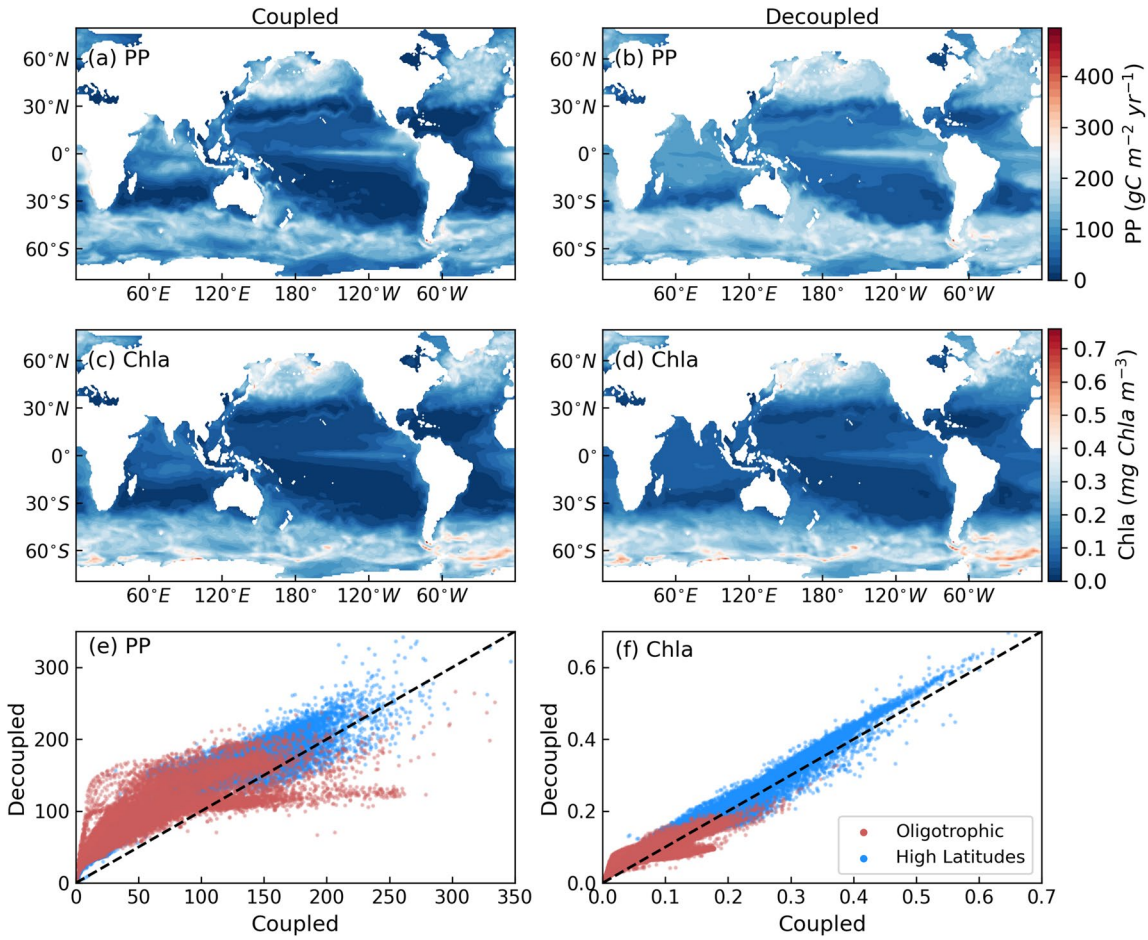

Figure 5. Comparison of coupled and decoupled simulations of Chla and primary production (PP). (a) simulated primary production of coupled model (0–55 m depth integrated, $gC\ m^{-2}\ yr^{-1}$), (b) simulated primary production of decoupled model (0–55 m depth integrated, $gC\ m^{-2}\ yr^{-1}$), (c) simulated Chla of coupled model (mean 0–55 m, $mg\ Chla\ m^{-3}$), (d) simulated Chla of decoupled model (mean 0–55 m, $mg\ Chla\ m^{-3}$), (e) Point by point comparison of primary production between coupled and decoupled simulations, (f) Point by point comparison of Chla between coupled and decoupled simulations. Oligotrophic regions are defined as regions between $40°S$ and $40°N$. High latitude regions are defined as regions beyond $40°S$ or $40°N$.

We asked what is the sensitivity of globally integrated primary production to the decoupling of nutrient and C at the cellular scale? Modeled global primary production of the coupled and decoupled simulations were 34.0 $Pg\ C \cdot yr^{-1}$ and 45.8 $Pg\ C \cdot yr^{-1}$ ($f_{e,j} = 0.7$) respectively — an increase of 35% (29%–38% over a range of plausible $f_{e,j}$, see Section 3.3 for more details). Satellite-derived estimates range between $44 - 57\ Pg\ C \cdot yr^{-1}$ with the mean of 50.7 $Pg\ C \cdot yr^{-1}$ (Carr et al., 2006; Field et al., 1998; Silsbe et al., 2016) suggesting that the decoupled estimate is potentially more plausible. However, there are large uncertainties underlying in both ocean color based and general circulation model based estimates of global primary production ranging from 35 to ~ 70 $Pg\ C \cdot yr^{-1}$ (Carr et al., 2006). We compared the spatial variations of primary production in the two 3D simulations (coupled and decoupled) against a suite of remote-sensing derived estimates of global-scale patterns and rates of primary production (Figures S5 and S6). But due to the large uncertainties of satellites estimates (e.g., differences between various remote sensing products), we could not quantitatively distinguish whether either coupled or decoupled simulation has more skill predicting primary production. The vertical profile of primary production does improve relative to observations (see Figures 4c and 4d) with the decoupled simulation.

The difference in primary production between decoupled and coupled simulations mainly lies in oligotrophic gyres where there is a low nutrient supply rate relative to the incoming light energy, as illustrated in Figure 5. The vertically integrated primary production at HOT and BATS in 3D decoupled simulation also increased by 40.2% and 42.7% respectively, similar with 1D simulations (Figure 4). The increase of primary

Table 2
Global Primary Production (Full Depth Integrated), Surface Exudation, DOC, Ratio of Exudation to Photosynthesis (REP), and Phytoplankton Stoichiometry (55 m Depth Integrated) in Different $f_{e,j}$ Scenarios

	Primary production	Exudation	DOC			
$f_{e,j}$	(Pg C/yr)	(Pg C/yr)	(Pg C)	REP	C:N	C:P
0	33.98	0.0	1.86	0.0	6.62	106.0
0.1	43.98	1.06	2.48	2.97%	10.03	160.49
0.3	44.48	3.31	2.58	9.13%	9.43	150.88
0.5	45.08	5.78	2.70	15.65%	8.79	140.67
0.7	45.82	8.54	2.83	22.66%	8.10	129.63
0.9	46.84	11.78	3.00	30.40%	7.33	117.27

Note. 0 in $f_{e,j}$ indicates the results of the coupled simulation.

production between 40°S and 40°N is 44.2% while in high latitude regions (beyond 40°S or 40°N) this increase is only 23.2%. The difference is most notable in the Atlantic subtropical gyres where macro-nutrients were most depleted in the simulations (NO_3 fields showed Figure S4a). The coupled simulation of primary production in subtropical gyres is too low relative to all the satellite-based products (Figure S6). The increased primary production in these regions in the decoupled simulation (Figures 5 and S6) suggests that the decoupling of carbon and nitrogen flow does indeed improve modeled primary production.

The difference in Chla between decoupled and coupled simulations is also most pronounced in the oligotrophic subtropical gyres. Chla decreases in the decoupled model relative to the coupled model because Chla synthesis is regulated by the ratio of photosynthesis rate and light harvesting rate resulting in a negative relationship with $P_{C,j}^{Sat}$ (see Equations S20 and S21). On a point-by-point basis, the simulations of Chla are modestly correlated with the climatology based on remote sensing (Figure S5, correlation coefficient 0.45) and has a much weaker variation (standard deviation less than half that) of the observed field. The two simulations are almost identical in this regard (Figure S5) so Chla comparisons do not discriminate.

3.3. Global-Scale Signatures of Excess Carbon Exudation

The mechanisms and controls on phytoplankton exudation still remain an open question. In these explorations we have assumed that excess photosynthate is produced when carbon fixation is in excess of growth potential and either accumulates in a "reserve," up to a maximum capacity, or is exuded. The fraction of excess photosynthesis that is exuded ($f_{e,j}$) cannot be determined from a priori (Equation 11) but in theory can vary between 0 and 1. In the results we have shown to this point we set $f_{e,j} = 0.7$ for both of the two classes of phytoplankton (based on criteria described below). However, $f_{e,j}$ likely varies between species, regions and over time. How this varies is beyond the scope of this study, but here we examine the sensitivity of $f_{e,j}$ by running 5 simulations with the decoupled model varying $f_{e,j}$ from 0.1, 0.3, 0.5, 0.7, and 0.9 (Table 2). The global exudation rate increased in proportion to $f_{e,j}$ while primary production remained at a similar level indicating that $f_{e,j}$ only affects exudation rates not photosynthesis rate. The increase of primary production between coupled and decoupled simulations mainly results from the decoupling of photosynthesis and biosynthesis. For the simulation where $f_{e,j} = 0.7$, the contribution of global exudation accounted for ~19% of the total labile/semi-labile DOC fluxes with the rest originating from death and sloppy feeding. However, the increase of DOC standing stock and the contribution of exudation will be even less to total DOC, as only labile/semi-labile DOC is resolve in the model which can be quickly used by heterotrophic bacteria. More importantly, none of these parameters are well constrained in the model, reflecting both the simplicity of the parameterizations, but also the challenge of a clear and quantitative interpretation of the mechanisms at laboratory work.

In the decoupled simulations ($f_{e,j} = 0.7$), the predicted surface exudation rate (0–55 m integral) is shown in Figure 6a and the predicted percentage of total C in the C reserve is shown is Figure 6b. As would be expected, the percentage of total phytoplankton carbon in the reserve pool shares a similar spatial pattern with surface exudation, reflecting regions where strong nutrient limitation and high photon fluxes coincide and in accord with previous experimental and modeling studies (Braakman, 2019; Flynn et al., 2008; Livanou et al., 2019; Szul et al., 2019). We quantified the ratio of exudation to photosynthesis (REP), defined as the percentage of total net photosynthesis released as exudates (shown in Figure 6c). REP is less than 15% in high latitude regions and greater than 50% in subtropical gyres. This pattern is broadly consistent with field studies that reported that REP less than 10% in productive regions with high nutrient concentration and up to 46% in less productive regions like oligotrophic subtropical gyres (Lagaria et al., 2013; Teira, Pazó, et al., 2001; Teira, Serret, & Fernández, 2001). Similarly, in laboratory cultures, REP has been observed to vary between 2% and 10% under nutrient-replete conditions and increase up to 60% in nutrient-deplete conditions (Myklestad, 2000).

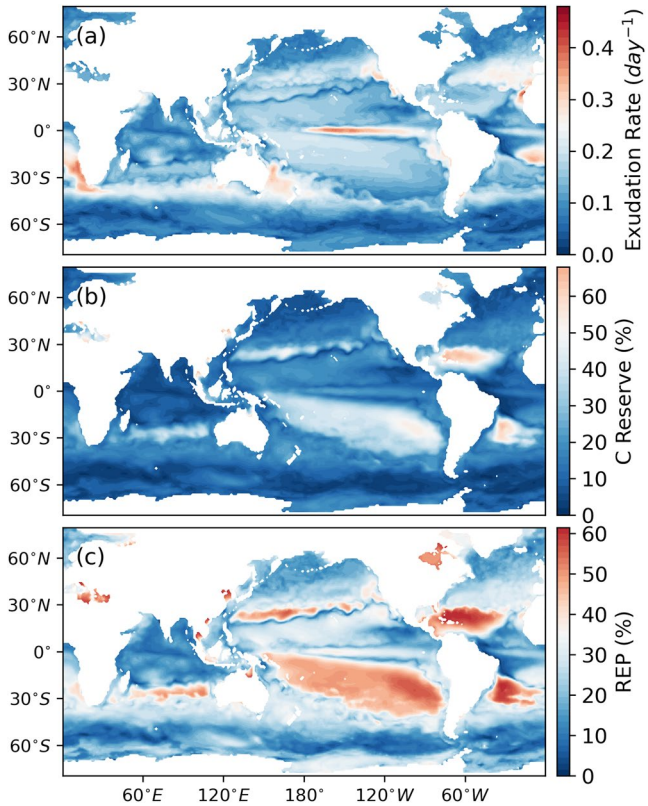

Figure 6. Global exudation rate, C reserve, and the ratio of exudation to photosynthesis patterns (55 m depth integrated). (a) simulated exudation rate (day^{-1}), (b) Percentage of total phytoplankton C in C reserve (%), (c) Ratio of exudation to photosynthesis (REP) (%).

By decoupling photosynthesis and biosynthesis and allowing extra C storage in cells, the decoupled model (Figure 2b) enables a flexible phytoplankton stoichiometry, which leads to a more dynamic and realistic meridional pattern of particulate stoichiometry (Figures 7, S7 and S8) with higher C:P and C:P in subtropical regimes (Martiny et al., 2014; Martiny, Pham, et al., 2013; Martiny, Vrugt, et al., 2013). We explored whether the global patterns of particulate C:N and C:P ratios could serve to constrain the value of $f_{e,j}$, which determines relative allocation to storage and exudation. However, there is unlikely to be a optimal value since $f_{e,j}$ is likely species specific and sensitive to the environment. The improvement of meridional phytoplankton stoichiometry originates more from the decoupling between photosynthesis and biosynthesis than a precise value of $f_{e,j}$.

4. Summary and Outlook

We have examined the consequences of the tight coupling of nutrient availability and photosynthesis in a commonly employed parameterization (Geider et al., 1997) for regional and global-scale carbon cycle simulations. The decoupling of these two processes significantly improved simulations of the vertical profile of subtropical primary productivity when compared to in situ observations. In global simulations, it increased integrated primary production by about one-third with the most impact in oligotrophic subtropical gyres where the original formulation with coupled processes consistently underestimated primary production relative to many satellite-based estimates. However, we note the large uncertainty in the large scale satellite based estimates (see e.g., Figure S5, Carr et al., 2006). In addition, other variations associated with regional changes in carbon demand not resolved here may also impact global productivity.

In order to explore the sensitivity of regional and global-scale simulations we have assumed either complete coupling or decoupling of photosynthesis/biosynthesis. It is likely that neither extreme is fully realistic and Geider et al. (1997) were clear about the uncertainty associated with the coupled assumption. There are numerous ways in which phytoplankton can accommodate light intensities greater than required to satisfy biosynthesis constraints, including the production of photo-protective pigments and photo-respiration (Halsey & Jones, 2015) which have not been considered here but could potentially reduce the importance of exudation. However, photo-respiration is significant only under the pressure of CO_2 depletion which should be minimal in this study (Beardall, 1989; Beardall et al., 2003; Wingler et al., 2000). Additionally, photo-inhibition and maintenance respiration are also not included in this study for model simplicity. We note that inclusion of these two processes would have little impact on the comparison of the two parameterizations but would indeed reduce the absolute predicted values of exudation. Despite the aforementioned limitations, this study still provides a clear indication of the sensitivity to two extreme possibilities and shows that they do have major implications for the simulation of global-scale productivity and the production of DOC. Most compellingly, the simulations demonstrate that the vertical profile of primary production in oligotrophic environments is significantly improved in the decoupled case, bringing the simulations into agreement with observed profiles of primary production and Chla at HOT and BATS. As a consequence we suggest that the decoupled approach is the better candidate for global carbon cycle simulations at present. In the global 3D simulation this new parameterization increased globally integrated, annual primary production by about a third. Such changes could have significant impact on how models capture the cycling of carbon in the upper ocean, and such processes may have an impact on their ability to capture inter-annual and longer term changes in the carbon cycle. We also note that the improvement in the vertical profile of simulations was more significant in the

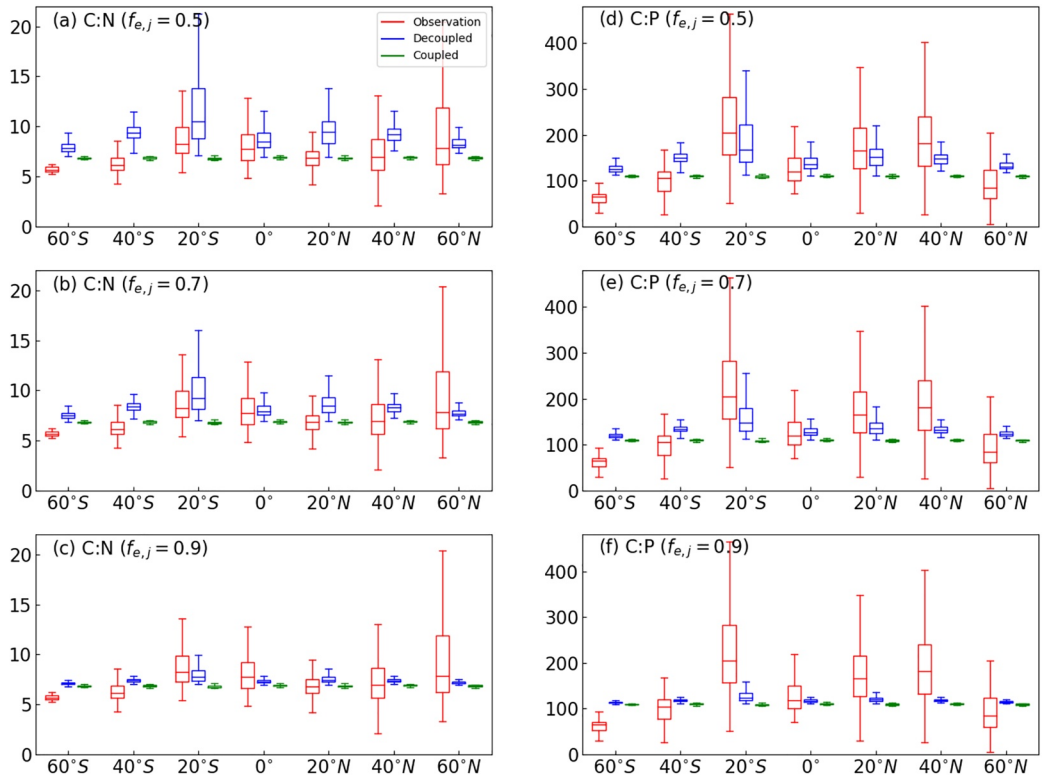

Figure 7. Particulate C:N and C:P ratios in observation (red), coupled simulation (green), and decoupled simulations (blue) with different $f_{e,j}$. (a–c) are C:N ratios with $f_{e,j} = 0.5, 0.7, 0.9$, (d–f) are C:P ratios with $f_{e,j} = 0.5, 0.7, 0.9$. The red bars of observations only contain a limited number of observation points while the blue and green bars of the simulations include all the grid points within each range. Observations used in this plot are from Martiny et al. (2014) which consists of 100,605 total measurements of particulate organic carbon, nitrogen, or phosphorus analyzed as part of 70 cruises or time-series.

1D simulation when vertically resolution is higher. As climate and carbon cycle models increase in both horizontal and vertical resolution with increasing computational resources, the issue will be more apparent.

Allocation of excess photosynthate to the reserve increases simulated C:N and C:P ratios of particulate matter, particularly in the subtropics. Depending on the choice of parameter values for the amount of carbon exuded versus stored, these increases in the subtropics brought the model more into line with observations (Martiny et al., 2014), and thus may provide an empirical, large-scale calibration. Allocation of all excess photosynthate to exudation would imply an additional source of DOC of more than 12 $Pg\ C\ yr^{-1}$. Allocation of all excess photosynthate to reserves would imply a global increase in C:N from 6.6:1 (Redfield Ratio) to greater than 10:1. A systematic and quantitative data-model synthesis might be employed to better constrain this allocation at the community level, though the complexities and uncertainties of DOC dynamics still cloud the development of suitable parameterizations. Additionally, here we used a uniform parameter $f_{e,j}$ for both types of phytoplankton to control the allocation of excess photosynthate which is likely to be species specific, and the biochemical composition and morphology of the cell could change exudation efficiency in response to environmental factors, for example phosphorus supply (Bertilsson et al., 2003).

In summary, we examined the consequence of decoupling photosynthesis and biosynthesis in the parameterization of photosynthesis employed in global biogeochemical models. We found that removing direct nutrient limitation to photosynthesis significantly improved the simulations of vertical profiles of primary production in the subtropical gyres and increased predicted global primary production by more than 30% relative to the case where photosynthesis and biosynthesis were tightly coupled. We explored the consequences of retention versus exudation of the excess photosynthate in the global simulations which improved the global patterns of C:N and C:P ratios in phytoplankton compared to the coupled model.

Data Availability Statement

The code and configurations of the models used in this paper can be found at https://doi.org/10.6084/m9.figshare.13564229.

Acknowledgments
The authors are grateful for the support by the Simons Collaboration on Ocean Processes and Ecology (SCOPE, 329108 to M. J. Follows and A. White) and Simons Collaboration on Computational Biogeochemical Modeling of Marine Ecosystems (CBIOMES, 549931 to M. J. Follows). Additional support is provided by the NSF to the HOT program (OCE-1756517 to A. White), the Human Frontiers Science Program (RGP0020/2016 to D. Sher). The authors thank the two anonymous reviewers whose comments and suggestions helped improve and clarify this manuscript. The authors also thank the dedicated efforts of the HOT and BATS teams who facilitated in situ sample collection.

References

Arrigo, K. R. (2005). Marine microorganisms and global nutrient cycles (Vol. 437). Nature Publishing Group. https://doi.org/10.1038/nature04159

Beardall, J. (1989). Photosynthesis and photorespiration in marine phytoplankton. *Aquatic Botany*, *34*(1–3), 105–130. https://doi.org/10.1016/0304-3770(89)90052-1

Beardall, J., Quigg, A., & Raven, J. A. (2003). Oxygen consumption: Photorespiration and chlororespiration. In A. W. D. Larkum, S. E. Douglas, & J. A. Raven (Eds.), *Photosynthesis in algae* (pp. 157–181). Dordrecht: Springer Netherlands. https://doi.org/10.1007/978-94-007-1038-2_8

Berman, T., & Holm-Hansen, O. (1974). Release of photoassimilated carbon as dissolved organic matter by marine phytoplankton. *Marine Biology*, *28*(4), 305–310. https://doi.org/10.1007/BF00388498

Bertilsson, S., Berglund, O., Karl, D. M., & Chisholm, S. W. (2003). Elemental composition of marine Prochlorococcus and Synechococcus: Implications for the ecological stoichiometry of the sea. *Limnology and Oceanography*, *48*(5), 1721–1731. https://doi.org/10.4319/lo.2003.48.5.1721

Bertlisson, S., Berglund, O., Pullin, M. J., & Chisholm, S. W. (2005). Release of dissolved organic matter by Prochlorococcus. *Vie et Milieu*, *55*(3–4), 225–232.

Bjørrisen, P. K. (1988). Phytoplankton exudation of organic matter: Why do healthy cells do it? (Vol. 33). John Wiley & Sons, Ltd. https://doi.org/10.4319/lo.1988.33.1.0151

Braakman, R. (2019). *Evolution of cellular metabolism and the rise of a globally productive biosphere*. https://doi.org/10.1016/j.freeradbiomed.2019.05.004

Braakman, R., Follows, M. J., & Chisholm, S. W. (2017). Metabolic evolution and the self-organization of ecosystems. *Proceedings of the National Academy of Sciences*, *114*(15), E3091–E3100. https://doi.org/10.1073/pnas.1619573114

Bruggeman, J., & Kooijman, S. A. (2007). A biodiversity-inspired approach to aquatic ecosystem modeling. *Limnology and Oceanography*, *52*(4), 1533–1544. https://doi.org/10.4319/lo.2007.52.4.1533

Cailliau, C., Claustre, H., Vidussi, F., Marie, D., & Vaulot, D. (1996). Carbon biomass, and gross growth rates as estimated from 14C pigment labelling, during photoacclimation in Prochlorococcus CCMP 1378. *Marine Ecology Progress Series*, *145*(1–3), 209–221. https://doi.org/10.3354/meps145209

Carr, M. E., Friedrichs, M. A., Schmeltz, M., Noguchi Aita, M., Antoine, D., Arrigo, K. R., & Yamanaka, Y. (2006). A comparison of global estimates of marine primary production from ocean color. *Deep-Sea Research Part II: Topical Studies in Oceanography*, *53*(5–7), 741–770. https://doi.org/10.1016/j.dsr2.2006.01.028

Cavender-Bares, K. K., Karl, D. M., & Chisholm, S. W. (2001). Nutrient gradients in the western North Atlantic Ocean: Relationship to microbial community structure and comparison to patterns in the Pacific Ocean. *Deep-Sea Research Part I: Oceanographic Research Papers*, *48*(11), 2373–2395. https://doi.org/10.1016/S0967-0637(01)00027-9

Clayton, S., Dutkiewicz, S., Jahn, O., & Follows, M. J. (2013). Dispersal, eddies, and the diversity of marine phytoplankton. *Limnology and Oceanography: Fluids and Environments*, *3*(1), 182–197. https://doi.org/10.1215/21573689-2373515

Colman, B. (1989). Photosynthetic carbon assimilation and the suppression of photorespiration in the cyanobacteria. *Aquatic Botany*, *34*(1–3), 211–231. https://doi.org/10.1016/0304-3770(89)90057-0

Dutkiewicz, S., Cermeno, P., Jahn, O., Follows, M. J., Hickman, A. A., Taniguchi, D. A., & Ward, B. A. (2020). Dimensions of marine phytoplankton diversity. *Biogeosciences*, *17*(3), 609–634. https://doi.org/10.5194/bg-17-609-2020

Dutkiewicz, S., Hickman, A. E., Jahn, O., Gregg, W. W., Mouw, C. B., & Follows, M. J. (2015). Capturing optically important constituents and properties in a marine biogeochemical and ecosystem model. *Biogeosciences*, *12*(14), 4447–4481. https://doi.org/10.5194/bg-12-4447-2015

Field, C. B., Behrenfeld, M. J., Randerson, J. T., & Falkowski, P. (1998). Primary production of the biosphere: Integrating terrestrial and oceanic components. *Science*, *281*(5374), 237–240. https://doi.org/10.1126/science.281.5374.237

Flynn, K. J. (2003). Modelling multi-nutrient interactions in phytoplankton; balancing simplicity and realism (Vol. 56). Elsevier. https://doi.org/10.1016/S0079-6611(03)00006-5

Flynn, K. J., Clark, D. R., & Xue, Y. (2008). Modeling the release of dissolved organic matter by phytoplankton. *Journal of Phycology*, *44*(5), 1171–1187. https://doi.org/10.1111/j.1529-8817.2008.00562.x

Follows, M. J., Dutkiewicz, S., Grant, S., & Chisholm, S. W. (2007). Emergent biogeography of microbial communities in a model ocean. *Science*, *315*(5820), 1843–1846. https://doi.org/10.1126/science.1138544

Garcia, H. E., Locarnini, R. A., Boyer, T. P., Antonov, J. I., Baranova, O. K., Zweng, M. M., & Johnson, D. R. (2018). World ocean atlas 2018, volume 4: Dissolved inorganic nutrients (phosphate, nitrate and and nitrate+nitrite, silicate) (Vol. 4). Retrieved from https://www.nodc.noaa.gov/OC5/woa18/pubwoa18.html

Geider, R. J., MacIntyre, H. L., & Kana, T. M. (1997). Dynamic model of phytoplankton growth and acclimation: Responses of the balanced growth rate and the chlorophyll a: Carbon ratio to light, nutrient-limitation and temperature. *Marine Ecology Progress Series*, *148*(1–3), 187–200. https://doi.org/10.3354/meps148187

Grossowicz, M., Roth-Rosenberg, D., Aharonovich, D., Silverman, J., Follows, M. J., & Sher, D. (2017). Prochlorococcus in the lab and in silico: The importance of representing exudation. *Limnology and Oceanography*, *62*(2), 818–835. https://doi.org/10.1002/lno.10463

Halsey, K. H., & Jones, B. M. (2015). Phytoplankton strategies for photosynthetic energy allocation. *Annual Review of Marine Science*, *7*(1), 265–297. https://doi.org/10.1146/annurev-marine-010814-015813

Hickman, A. E., Dutkiewicz, S., Williams, R. G., & Follows, M. J. (2010). Modelling the effects of chromatic adaptation on phytoplankton community structure in the oligotrophic ocean. *Marine Ecology Progress Series*, *406*, 1–17. https://doi.org/10.3354/meps08588

Karl, D. M., & Church, M. J. (2014). Microbial oceanography and the Hawaii ocean time-series programme (Vol. 12). https://doi.org/10.1038/nrmicro3333

Kulk, G., de Poll, W. H., Visser, R. J., & Buma, A. G. (2011). Distinct differences in photoacclimation potential between prokaryotic and eukaryotic oceanic phytoplankton. *Journal of Experimental Marine Biology and Ecology*, *398*(1–2), 63–72. https://doi.org/10.1016/j.jembe.2010.12.011

Lagaria, A., Psarra, S., Gogou, A., Tuğrul, S., & Christaki, U. (2013). Particulate and dissolved primary production along a pronounced hydrographic and trophic gradient (Turkish Straits System-NE Aegean Sea). *Journal of Marine Systems*, *119–120*, 1–10. https://doi.org/10.1016/j.jmarsys.2013.02.009

Letelier, R. M., Dore, J. E., Winn, C. D., & Karl, D. M. (1996). Seasonal and interannual variations in photosynthetic carbon assimilation at station ALOHA. *Deep-Sea Research Part II: Topical Studies in Oceanography*, *43*(2–3), 467–490. https://doi.org/10.1016/0967-0645(96)00006-9

Letelier, R. M., White, A. E., Bidigare, R. R., Barone, B., Church, M. J., & Karl, D. M. (2017). Light absorption by phytoplankton in the North Pacific subtropical gyre. *Limnology and Oceanography*, *62*(4), 1526–1540. https://doi.org/10.1002/lno.10515

Livanou, E., Lagaria, A., Psarra, S., & Lika, K. (2019). A DEB-based approach of modeling dissolved organic matter release by phytoplankton. *Journal of Sea Research*, *143*, 140–151. https://doi.org/10.1016/j.seares.2018.07.016

López-Sandoval, D. C., Rodríguez-Ramos, T., Cermeño, P., & Marañón, E. (2013). Exudation of organic carbon by marine phytoplankton: Dependence on taxon and cell size. *Marine Ecology Progress Series*, *477*, 53–60. https://doi.org/10.3354/meps10174

Luo, C., Mahowald, N., Bond, T., Chuang, P. Y., Artaxo, P., Siefert, R., & Schauer, J. (2008). Combustion iron distribution and deposition. *Global Biogeochemical Cycles*, *22*(1), GB1012. https://doi.org/10.1029/2007GB002964

Mackey, K. R., Paytan, A., Grossman, A. R., & Bailey, S. (2008). A photosynthetic strategy for coping in a high-light, low-nutrient environment. *Limnology and Oceanography*, *53*(3), 900–913. https://doi.org/10.4319/lo.2008.53.3.0900

Malmstrom, R. R., Coe, A., Kettler, G. C., Martiny, A. C., Frias-Lopez, J., Zinser, E. R., & Chisholm, S. W. (2010). Temporal dynamics of Prochlorococcus ecotypes in the Atlantic and pacific oceans. *ISME Journal*, *4*(10), 1252–1264. https://doi.org/10.1038/ismej.2010.60

Marañón, E., Cermeño, P., López-Sandoval, D. C., Rodríguez-Ramos, T., Sobrino, C., Huete-Ortega, M., et al. (2013). Unimodal size scaling of phytoplankton growth and the size dependence of nutrient uptake and use. *Ecology Letters*, *16*(3), 371–379. https://doi.org/10.1111/ele.12052

Marshall, J., Adcroft, A., Hill, C., Perelman, L., & Heisey, C. (1997). A finite-volume, incompressible navier stokes model for, studies of the ocean on parallel computers. *Journal of Geophysical Research*, *102*(C3), 5753–5766. https://doi.org/10.1029/96JC02775

Martin, P., Dyhrman, S. T., Lomas, M. W., Poulton, N. J., & Van Mooy, B. A. (2014). Accumulation and enhanced cycling of polyphosphate by Sargasso sea plankton in response to low phosphorus. *Proceedings of the National Academy of Sciences of the United States of America*, *111*(22), 8089–8094. https://doi.org/10.1073/pnas.1321719111

Martiny, A. C., Pham, C. T., Primeau, F. W., Vrugt, J. A., Moore, J. K., Levin, S. A., & Lomas, M. W. (2013). Strong latitudinal patterns in the elemental ratios of marine plankton and organic matter. *Nature Geoscience*, *6*(4), 279–283. https://doi.org/10.1038/ngeo1757

Martiny, A. C., Vrugt, J. A., & Lomas, M. W. (2014). Concentrations and ratios of particulate organic carbon, nitrogen, and phosphorus in the global ocean. *Scientific Data*, *1*(1), 1–7. https://doi.org/10.1038/sdata.2014.48

Martiny, A. C., Vrugt, J. A., Primeau, F. W., & Lomas, M. W. (2013). Regional variation in the particulate organic carbon to nitrogen ratio in the surface ocean. *Global Biogeochemical Cycles*, *27*(3), 723–731. https://doi.org/10.1002/gbc.20061

McGillicuddy, D. J. (2016). Mechanisms of physical-biological-biogeochemical interaction at the oceanic mesoscale. *Annual Review of Marine Science*, *8*(1), 125–159. https://doi.org/10.1146/annurev-marine-010814-015606

Mills, M. M., & Arrigo, K. R. (2010). Magnitude of oceanic nitrogen fixation influenced by the nutrient uptake ratio of phytoplankton. *Nature Geoscience*, *3*(6), 412–416. https://doi.org/10.1038/ngeo856

Myklestad, S. M. (2000). Dissolved organic carbon from phytoplankton. In *Marine chemistry* (pp. 111–148). Springer-Verlag. https://doi.org/10.1007/10683826{_}5

Roth-Rosenberg, D., Aharonovich, D., Omta, A. W., Follows, M. J., & Sher, D. (2021). Dynamic macromolecular composition and high exudation rates in Prochlorococcus. *Limnology and Oceanography*, *66*(5), 1759–1773. https://doi.org/10.1002/lno.11720

Sarmento, H., Morana, C., & Gasol, J. M. (2016). Bacterioplankton niche partitioning in the use of phytoplankton-derived dissolved organic carbon: Quantity is more important than quality. *ISME Journal*, *10*(11), 2582–2592. https://doi.org/10.1038/ismej.2016.66

Schartau, M., Engel, A., Schröter, J., Thoms, S., Völker, C., & Wolf-Gladrow, D. (2007). Modelling carbon overconsumption and the formation of extracellular particulate organic carbon. *Biogeosciences*, *4*(4), 433–454. https://doi.org/10.5194/bg-4-433-2007

Silsbe, G. M., Behrenfeld, M. J., Halsey, K. H., Milligan, A. J., & Westberry, T. K. (2016). The Cafe model: A net production model for global ocean phytoplankton. *Global Biogeochemical Cycles*, *30*(12), 1756–1777. https://doi.org/10.1002/2016GB005521

Steinberg, D. K., Carlson, C. A., Bates, N. R., Johnson, R. J., Michaels, A. F., & Knap, A. H. (2001). Overview of the US JGOFS Bermuda Atlantic time-series study (BATS): A decade-scale look at ocean biology and biogeochemistry. *Deep-Sea Research Part II: Topical Studies in Oceanography*, *48*(8–9), 1405–1447. https://doi.org/10.1016/S0967-0645(00)00148-X

Szul, M. J., Dearth, S. P., Campagna, S. R., & Zinser, E. R. (2019). Carbon fate and flux in Prochlorococcus under nitrogen limitation. *mSystems*, *4*(1). https://doi.org/10.1128/msystems.00254-18

Talmy, D., Blackford, J., Hardman-Mountford, N. J., Polimene, L., Follows, M. J., & Geider, R. J. (2014). Flexible C: N ratio enhances metabolism of large phytoplankton when resource supply is intermittent. *Biogeosciences*, *11*(17), 4881–4895. https://doi.org/10.5194/bg-11-4881-2014

Teira, E., Pazó, M. J., Serret, P., & Fernández, E. (2001). Dissolved organic carbon production by microbial populations in the Atlantic Ocean. *Limnology and Oceanography*, *46*(6), 1370–1377. https://doi.org/10.4319/lo.2001.46.6.1370

Teira, E., Serret, P., & Fernández, E. (2001). Phytoplankton size-structure, particulate and dissolved organic carbon production and oxygen fluxes through microbial communities in the NW Iberian coastal transition zone. *Marine Ecology Progress Series*, *219*, 65–83. https://doi.org/10.3354/meps219065

Thompson, A. W., van den Engh, G., Ahlgren, N. A., Kouba, K., Ward, S., Wilson, S. T., & Karl, D. M. (2018). Dynamics of Prochlorococcus diversity and photoacclimation during short-term shifts in water column stratification at station ALOHA. *Frontiers in Marine Science*, *5*, 488. https://doi.org/10.3389/fmars.2018.00488

Thornton, D. C. (2014). Dissolved organic matter (DOM) release by phytoplankton in the contemporary and future ocean. *European Journal of Phycology*, *49*(1), 20–46. https://doi.org/10.1080/09670262.2013.875596

Vallino, J. J. (2000). Improving marine ecosystem models: Use of data assimilation and mesocosm experiments. *Journal of Marine Research*, *58*(1), 117–164. https://doi.org/10.1357/002224000321511223

Ward, B. A., Dutkiewicz, S., Jahn, O., & Follows, M. J. (2012). A size-structured food-web model for the global ocean. *Limnology and Oceanography*, *57*(6), 1877–1891. https://doi.org/10.4319/lo.2012.57.6.1877

Ward, B. A., & Follows, M. J. (2016). Marine mixotrophy increases trophic transfer efficiency, mean organism size, and vertical carbon flux. *Proceedings of the National Academy of Sciences*, *113*(11), 2958–2963. https://doi.org/10.1073/pnas.1517118113

White, A. E., Letelier, R. M., Whitmire, A. L., Barone, B., Bidigare, R. R., Church, M. J., & Karl, D. M. (2015). Phenology of particle size distributions and primary productivity in the North Pacific subtropical gyre (Station ALOHA). *Journal of Geophysical Research: Oceans*, *120*(11), 7381–7399. https://doi.org/10.1002/2015JC010897

Wingler, A., Lea, P. J., Quick, W. P., & Leegood, R. C. (2000). Photorespiration: Metabolic pathways and their role in stress protection. In Philosophical transactions of the royal society b: Biological sciences (Vol. 355, pp. 1517–1529). Royal Society. https://doi.org/10.1098/rstb.2000.0712

Wunsch, C., & Heimbach, P. (2007). Practical global oceanic state estimation. *Physica D: Nonlinear Phenomena*, *230*(1–2), 197–208. https://doi.org/10.1016/j.physd.2006.09.040

Xiu, P., & Chai, F. (2014). Connections between physical, optical and biogeochemical processes in the Pacific ocean. *Progress in Oceanography*, *122*, 30–53. https://doi.org/10.1016/j.pocean.2013.11.008